Elucidating plasma dynamics in Hasegawa-Wakatani turbulence by information geometry

Anderson, J., Kim, E., Hnat, B. & Rafiq, T.

Original citation & hyperlink:
Anderson, J, Kim, E, Hnat, B & Rafiq, T 2020, 'Elucidating plasma dynamics in Hasegawa-Wakatani turbulence by information geometry', Physics of Plasmas, vol. 27, no. 2, 022307.
https://dx.doi.org/10.1063/1.5122865

DOI 10.1063/1.5122865
ISSN 1070-664X
ESSN 1089-7674

Publisher: American Institute of Physics

Elucidating plasma dynamics in Hasegawa-Wakatani turbulence by information geometry

Johan Anderson,[1, a)] Eun-jin Kim,[2] Bogdan Hnat,[3] and Tariq Rafiq[4]

[1)] *Department of Earth and Space Sciences, Chalmers University of Technology, SE-412 96 Göteborg, Sweden*

[2)] *School of Mathematics and Statistics, University of Sheffield, Sheffield S3 7RH, United Kingdom; Fluid and Complex Systems Research Centre, Coventry University, CV1 2TT, United Kingdom*

[3)] *Department of Physics, University of Warwick, Coventry, CV4 7AL, United Kingdom*

[4)] *Department of Mechanical Engineering and Mechanics, Lehigh University, Bethlehem, PA 18015, USA*

(Dated: 1 February 2020)

The impact of adiabatic electrons on drift-wave turbulence, modelled by the Hasegawa-Wakatani equations, is studied using information length. Information length is a novel theoretical method for measuring distances between statistical states represented by different probability distribution functions (PDFs) along the path of a system and represents the total number of statistically different states that a system evolves through in time. Specifically, the time-dependent PDFs of turbulent fluctuations for a given adiabatic index A is computed. The changes in fluctuation statistics are then quantified in time by using information length. The numerical results provide time traces exhibiting intermittent plasma dynamics, and such behaviour is identified by a rapid change in the information length. The effects of A are discussed.

PACS numbers: 52.35.Ra, 52.25.Fi, 52.35.Mw, 52.25.Xz

Keywords: Hasegawa-Wakatani drift waves, stochastic theory, information geometry, time series analysis

[a)]Electronic mail: anderson.johan@gmail.com.

I. INTRODUCTION

Turbulence is ubiquitous in nature, and is of fundamental importance to many space and laboratory plasma systems. In magnetically confined (MC) plasmas, turbulent fluctuations in plasma potential, density and temperature cause elevated transport compared to classical predictions[1]. In MC plasmas, a large radial gradient is present resulting in a strong anisotropy between parallel and perpendicular length scales. The non-adiabatic electron response is a crucial component of their dynamics.

Investigations of this turbulent transport is an outstanding topic in fusion plasma research. Qualitative understanding can be obtained by studying reduced models, such as Hasegawa - Mima (HM) or the Hasegawa - Wakatani (HW) equations[1–10]. These models are more amenable to analytical elucidations as well as detailed numerical predictions. The HM and HW equations include fixed electron pressure gradient, which provides a driving mechanism for drift waves. These waves become unstable on the gyro-radius scale in the presence of parallel electron resistivity, present in the HW model. Non-linear interactions of large amplitude drift-waves leads to a turbulent state. This turbulence is quasi-2D, that is the energy condensates on large scales, hence the system evolves from random perturbations on small scales to an ordered state dominated by large-scale structures where the average size of a structure depends on the adiabatic parameter A. The ability to associate certain transport characteristics with particular physics of the model elucidates experimental results, as well as predictions from quantitative but more complex counterparts such as gyrokinetic models. In particular, HW model[4–9] is in an intermediate regime between adiabatic and hydrodynamic electrons, allowing the electrons to dynamically and self-consistently determine the relation between the density and the electrostatic potential through the turbulence.

Recently, the need to investigate large scale transport events such as bursts, streamers and blobs have been recognized[11–17]. These intermittent events are characterized by a bursty temporal structure and radial coherence. The Probability Distribution Functions (PDFs) of fluxes associated with these events have elevated tails compared to a Gaussian distribution, which can be a manifestation of large events or coherent structures mediating transport[13]. This statistical intermittency is quantified by higher order cumulants of the PDFs (e.g.

skewness and kurtosis)[18,19]. However, a key dynamical feature of magnetically confined plasma includes a different kind of structure, which is radially localized while extended in the poloidal direction[18–21]. These are known as zonal flows. Zonal flows are generated by the small scale turbulence and may act in a self-regulating manner and govern the saturation of the drift waves[22–25]. Theoretical models have previously successfully predicted the functional form of the PDF tail for the electrostatic fluctuations described by drift turbulence models[18,19].

Understanding the time evolution of in and out of equilibrium systems is one of the major goals in statistical mechanics. One of the possible options is to work with the different metrics for the thermodynamic length[26–31] and the information length[32–37] which is a generalisation of the thermodynamic length to non-equilibrium systems.

The thermodynamic length concerns comparing two PDFs and quantifies the difference between them by the shortest distance between the two by endowing a phase space with a Riemannian metric. Interestingly, one possible choice is to use the PDFs to construct the Fisher information metric[32,33]. This metric gives a novel methodology to measure distance in statistical space. Other popular statistical measures such as "relative entropy" or "Jensen divergence" also concern comparing two PDFs (e.g. at two different times).

When a PDF continuously changes with time, the information length measures the total number of different statistical states that a system passes through in time[32–37]. Therefore, the information length between the two PDFs at two different times can take any arbitrary value depending on a path between the two PDFs. As an example, let us consider that a system starting from its initial state at time 0 returns to its initial state at time t after undergoing temporal changes. The final state at time t and the initial state at time 0 are then identical. However, the information length at time t is non-zero since it captures the evolution of a system between the initial and final states. In comparison, the relative entropy or Jensen divergence between the initial and final states is zero.

A unique specialty of the information length is this path-dependence, permitting us to quantify the difference in the dynamics between two time points by measuring the distance that a system travels in between. The path dependence of the information length was shown to be useful for understanding the dynamical system, in particular, attractor structure. Hes-

eltine & Kim[37] compared the information length, relative entropy, Jensen divergence, etc and show that it was only the information length that captures a linear geometry of a linear Ornstein–Uhlenbeck process by a linear relation between the information length (in the long time limit) and the mean position of an initial Gaussian PDF[37]. The information length constitutes a geometric methodology to understand stochastic processes such as dynamic phase transition[34]. In fusion plasmas, it can be especially useful for understanding memory and hysteresis. We note that how the hysteresis is captured by the information length was studied in simpler models[34,38,39] by comparing forward and backward processes in 0D Ginzberg-Landau model with off-critical[34] and on-critical quenching[38] and logistic models[39]. Specially, in these models, to investigate the path-dependence and asymmetry of the information change under the time reversal $t \to -t$, the forward and back processes were chosen such that a PDF at $t = 0$ (as $t \to \infty$) for the forward process is identical to the PDF of the backward process as $t \to \infty$ (at $t = 0$). Drastically different behaviour of $\mathcal{E}$ and $\mathcal{L}$ as well as the evolution of time-dependent PDFs in the forward and backward processes were discussed in detail.

In this work, we investigate quasi-stationary time series of the electrostatic potential and corresponding vorticity (poloidally averaged (zonal part) and sampled at different radial points) from the HW simulations. We compute the information length $\mathcal{L}$, show examples of the time evolution of the PDFs and discuss implications and possible events in the time traces. A special attention is paid to the effects of the adabaticity parameter A and the radial position.

The paper is organized as follows. The HW model is described in Section II and the statistical analysis with interpretation methods are explained in Section III. The results are presented for electrostatic potential, vorticity and flux in Section IV, V and VI, respectively. The paper is concluded with a discussion in Section VII.

II. HASEGAWA - WAKATANI MODEL

As noted previously, the Hasegawa-Wakatani system of equations (HW) provide a model that has frequently been employed to study transport processes in magnetically confined

(MCF) plasma[4]. There exist quantitatively better and increasingly complex models, however studies of HW offers an alternative where sampling of long time series data and the time evolution of the PDFs can be monitored and calculated. These numerical simulations based on HW capture the key elements of MCF plasma dynamics: drift instability due to non-adiabatic electron response, onset of drift turbulence and the self-organisation of plasma into zonal flows.

The HW describes low frequency ($\omega \ll \omega_{ci}$, where ω_{ci} is the ion gyro frequency) fluctuations of the density n and the electrostatic potential ϕ, in the presence of the constant background density gradient, parallel electron resistivity and for a small ion-electron temperature ratio ($T_i/T_e \ll 1$). In the presence of axisymmetric zonal flows with poloidal wave number $m = 0$, which do not contribute to the parallel currents, the HW is in the two dimensional form[5–8]:

$$\frac{\partial n}{\partial t} = -\kappa \frac{\partial \phi}{\partial y} + A(\tilde{\phi} - \tilde{n}) + [n, \phi] + D\nabla^2 n, \tag{1}$$

$$\frac{\partial}{\partial t}\nabla^2 \phi = A(\tilde{\phi} - \tilde{n}) + [\nabla^2 \phi, \phi] + \mu\nabla^2(\nabla^2 \phi), \tag{2}$$

where total fluctuating fields n and ϕ consist of turbulent parts, $\tilde{n}$, $\tilde{\phi}$, and zonal fluctuations $\langle n \rangle$ and $\langle \phi \rangle$. That is, $n = \tilde{n} + \langle n \rangle$ and $\phi = \tilde{\phi} + \langle \phi \rangle$. In the extended HW model, a variation in the field and density is taken into account however for simplicity only a density gradient is included in the present work. The poloidal averages are denoted by the angular brackets $\langle \dots \rangle$, which in the slab model simply indicate integration along the poloidal line at a given radial location:

$$\langle f \rangle = \frac{1}{L_y} \int_0^{L_y} f dy. \tag{3}$$

The nonlinear advection terms are expressed as Poisson brackets $[A, B] = \partial A/\partial x.\partial B/\partial y - \partial A/\partial y.\partial B/\partial x$. In both equations physical quantities have been normalized using $e\phi/T_e \to \phi$, $n/n_0 \to n$, $\omega_{ci}t \to t$ and $(x, y)/\rho_s \to (x, y)$. Standard notation is used for other quantities: T_e is the electron temperature, ω_{ci} is the ion gyrofrequency, and $\rho_s = \sqrt{m_i T_e}/eB$ is the hybrid Larmor radius. Dissipation terms of the form $\nabla^2\phi$ are added to the equations for numerical stability, where D and μ are dissipation coefficients. The dissipation coefficients have physical interpretations where D is identified with the cross-field ambipolar diffusion and μ is the ion perpendicular viscosity where $D = 0.01$ and $\mu = 0.01$. The x and y directions are

identified with the radial and poloidal directions in a tokamak, respectively, and the magnetic field is assumed to point in the z direction. We assume that $\kappa = -\partial \ln(n_0)/\partial x$ is the characteristic spatial scale determines the background density profile $n_0(x) = \exp(-\kappa x)$. In Eqs. (1)-(2), there is a free parameter A that controls the strength of the resistive coupling between n and ϕ through the parallel current,

$$A = \frac{T_e k_{||}^2}{n_0 e^2 \eta \omega_{ci}} \tag{4}$$

where η is electron resistivity and $k_{||}$ is the parallel wave-number. This so-called the adiabaticity parameter A determines the degree to which electrons can move rapidly along the magnetic field lines and establish a perturbed Boltzmann density response. Note that this particular model is often referred to as the modified HW model due to coupling only on the fluctuations. There exist two limits of interest for the HW system and it approaches different regimes in the limits of $A \to 0$ and $A \to \infty$. When $A \to \infty$ and $n \to \phi$ (that is density fluctuations become enslaved to the electrostatic potential fluctuations), the HW become identical to a one field indirectly forced Charney-Hasegawa-Mima equation[2,3]. In the opposite limit $A \to 0$ the equation becomes equivalent to the incompressible Euler equation in 2D. A finite, non-zero A yields a growth rate causing a random stirring that prevents the vorticity from decaying to zero as is the usual case with the unforced Navier-Stokes. Note that there are both stable, unstable waves and non-modal solutions present in the system.

The equations (1) and (2) were solved numerically on a square grid of size $L = 40$ (units of ρ_s) with spatial resolution of 256×256 grid points using periodic boundary conditions. Note that, in Eq. (1) and (2) κ is independent of x and thus the system is symmetric and radially homogeneous. It is well known that the final stage of the HW evolution is dominated by zonal flows. In real laboratory plasmas and in 3D simulations, the poloidal damping of zonal flows enforces a certain level of energy equipartition between turbulence and zonal flows. Equipartition in our simulations is enforced by applying the following algorithm. We modify the decomposition of fluctuations so that each fluctuating quantity $Q = \tilde{Q} + \gamma\langle Q \rangle$ ($Q = n, \phi$), that is we multiply each poloidally averaged zonal flow component by factor γ. In each step of the simulation we monitor the kinetic energy of zonal flows

$$\langle E \rangle_K \equiv \frac{1}{2} \int \left(\frac{\partial \langle \phi \rangle}{\partial x} \right)^2 dV, \tag{5}$$

and its turbulent counterpart, given by

$$E_K \equiv \frac{1}{2}\int \left(\nabla\tilde{\phi}\right)^2 dV. \tag{6}$$

If at any time step $\langle E\rangle_K > E_K$, we set $\gamma = \sqrt{E_K/\langle E\rangle_K}$, otherwise we set $\gamma = 1.0$[8]. Note that this algorithm introduces an indirectly time dependent decomposition.

We perform three simulations varying the adiabaticity $A = 0.25$, 1.0 and 2.0, which capture three distinct dynamical regimes for the HW system (For each simulation, the value of A is fixed.). We examine poloidally averaged potential and vorticity i.e. the zonal components as defined by Eq. (3), where the data is collected in ten evenly spaced radial locations starting from location $x = 20$ and ending at $x = 200$. However, in the following, we present the results for the four radial points $x = 40, 80, 120, 160$.

III. TIME DEPENDENT PDFS AND INFORMATION LENGTH

For simplicity, let us consider a stochastic variable x with time-dependent PDF $p(x,t)$. When we know the control parameters λ^i that determine the PDF, we can calculate the Fisher-Information metric g_{ij}

$$g_{ij} = \int dx p(x,t) \frac{\partial \log p(x,t)}{\partial \lambda^i} \frac{\partial \log p(x,t)}{\partial \lambda^j}. \tag{7}$$

Note that the function $p(x,t)$ determines the probability of the system to be in state x at time t. Based on this metric tensor, we can write down the information length[32–35] as

$$\mathcal{L} = \int_0^\tau dt \sqrt{\frac{d\lambda^i}{dt} g_{ij} \frac{d\lambda^j}{dt}}. \tag{8}$$

The distance in Eq. (8) is measured by the difference between consecutive PDFs where the difference in PDFs gives a measure of the statistical distance. The evolution of a system can then be envisioned as the trajectory in the probability space where the distance/metric at different times is provided by the statistical distance. The information length is proportional to the time integral of the square root of the infinitesimal relative entropy[36].

In general, even when we do not know control parameters that govern PDFs, we can calculate the information length[32–36] by following the main two steps, computing the dynamic

time unit $\tau(t)$ and the total time in this unit. The dynamic time is the characteristic time scale over which $p(x,t)$ temporally changes on average at time t. The second step involves computation of the total elapsed time in units of this $\tau(t)$. Specifically, the dynamic time $\tau(t)$ is related to the second moment $\mathcal{E}$ (as can be inferred from combining Eqs. (8) and (7)) and can be computed as

$$\mathcal{E} = \frac{1}{\tau(t)^2} = \int dx \frac{1}{p(x,t)} \left(\frac{\partial p(x,t)}{\partial t} \right)^2 . \tag{9}$$

τ in Eq. (9) quantifies the correlation time over which the (dimensionless) information changes. The information length $\mathcal{L}(t)$ then follows[32],

$$\mathcal{L}(t) = \int_0^t \frac{ds}{\tau(s)} = \int_0^t ds \sqrt{\int dx \frac{1}{p(x,s)} \left(\frac{\partial p(x,s)}{\partial s} \right)^2} . \tag{10}$$

Note that none of the PDFs is identically zero, which would lead to a singularity in (10). The information length is dimensionless and represents the total different number of states between the initial and final times, 0 and t respectively, and establishes a distance between the initial and final PDFs in the statistical space. The simplest case elucidating this principle is a Gaussian distribution, statistically distinguishable states are determined by the standard deviation, which increases with the level of fluctuations.

Specifically, for a Gaussian PDF, a statistically different state is obtained due to the change in the mean value (the peak position of a PDF) or due to the change in the standard deviation (the width of a PDF). Physically, the former (mean value change) is due to the work while the latter (standard deviation change) is due to the entropy change. More technically, for the information length, the mean value change is to be normalized by the smallest scale (standard deviation) as the width of a Gaussian PDF gives the uncertainty (error) in measuring the mean position, and thus the smallest scale. The information length was shown to be proportional to the time integral of the square root of the infinitesimal relative entropy[36].

In the analysis of HW we focus on the time traces (averaged in the y-direction i.e. the zonal component) at four equidistant radial points located at $x = 40, 80, 120, 160$. The original simulation data sets are sampled to yield a more amenable data set that consists of typically 5×10^5 entries, which corresponds to typically a few hundreds eddy turnover

times. Thus, we employ the same analysis method for the electrostatic potential, vorticity and flux for all different values of the adiabaticity parameter (A) from 0.25, 1.00 and 2.00. We present all cases in turn comparing the results for each value of adiabaticity index A starting with the potentials, and PDFs and then finally the information length.

IV. RESULTS FOR POTENTIAL WITH VARYING ADIABATICITY

In this section the results of the analysis is presented. We start with a few observations from the simulations and the effect of the adiabaticity index A. We recall that small adiabaticity corresponds to Euler like dynamics and high adiabaticity HM limit, respectively. In Figure (1) the time traces of the potentials at the radial positions $(40, 80, 120, 160)$ are presented for $A = 0.25, 1.00$ and 2.00. These are the evolution of the potentials averaged over the poloidal direction (zonal component) and show considerable fluctuations over time. There are some significant differences between the three regimes described by different adiabaticity. For small adiabaticity ($A = 0.25$) there are several superimposed fluctuations on different time scales clearly visible whereas for larger adiabaticity fluctuations on a larger time scale seem to be of importance.

Interestingly, also the fluctuation levels decrease as the adiabaticity is increased corresponding to the different regimes. Specifically, for $A = 0.25$, the time traces of the potentials at the different radial positions span a similar interval between -10 and 8 with the similar statistical property (e.g. standard deviation) (results not shown). As A increases, the different behaviour at the different x becomes noticeable. For instance, for $A = 2$, the absolute values of ϕ for the red and purple lines ($x = 80$ and 160) are mostly smaller than those for the blue and yellow lines ($x = 40$ and $x = 120$). This indicates that there is a difference in the dynamics between ($x = 40$ and $x = 120$) and ($x = 80$ and $x = 160$) and could be an indication of the periodic character of the boundary. The dynamics will be quantified by computing PDFs at the corresponding radial points comparing the time evolution of these PDFs.

We note that bin length affects the results of our PDFs. Since we are interested in the effects of coherent structures (zonal potential or vorticity) on time-dependent PDFs, we

obtain time-dependent statistics by using a bin length of 10000 times the time resolution of the simulation that is longer than the eddy-turn over time (several tens of the time resolution of the simulation) but shorter than the time-scale of zonal potential or vorticity. Specifically, we construct our PDFs by using a time window of blocks of 10000 consecutive values without overlap of the windows, where each PDF span a few hundred eddy turnover times. An example of the time evolution of the PDFs are shown in Figure (2). The large fluctuations are clearly visible in the rather wide (large standard deviation) PDFs however also the large difference in mean is clearly visible. The information length assesses the distance between distributions at different instances in time along the path. Note that it is only an equilibrium distribution function that can be constructed from linear combinations of the non-linear invariants of the starting HW equations (after averaged over a sufficiently long time scale), and our systems are not in such an equilibrium with time-dependent PDFs.

Figure 3 presents the information length (log scale) computed for the radial positions (40, 80, 120, 160) with adiabaticity (A) as a parameter. We observe that the information length is monotonically increasing in time although at different rates. Note that, the information length saturates at a constant (stationary) value only when the PDFs are independent of time and that the expression for $1/\tau$ in Eq. (9) is non-negative and thus the information length which is the time integral of $1/\tau$ is a non-decreasing function of time. Interestingly, the fast fluctuation visible for $A = 0.25$ leads to a smaller information length as a function time compared with the case of the slower fluctuation for $A = 2.00$. This is because of a much higher fluctuation level and thus much higher uncertainty for $A = 0.25$ than for $A = 2.00$. We also mote that PDFs are dependent on the bin sizes – we have performed a sensitivity study using bin sizes of $500, 1000, 5000$ and 10000 to check that the resulting PDFs are rather stable for the larger bin size. Consequently, the information length is naturally dependent on the resolution. However we have confirmed a small variation in the information length over the bin size for all tested cases.

Moreover, it is noted that in Figure 1 for $A = 0.25$ there is a variation on a longer time scale and halfway through the simulation the potential flips from the negative side to the positive and vice versa on a short time whereas this behaviour is not found for higher adiabaticity on the same time scale. However, this is not immediately visible in Figure 3,

thus a more in-depth assessment is called for.:

For a close examination, the information length for $A = 0.25$ is displayed on a linear scale in Figure 4. Overall, we observe a linear increase in the information length. However, the rate of increase of the information length varies significantly. Since the slope of the information length is $1/\tau$ in Eq. (9), we look at how $1/\tau^2 = \mathcal{E}$ changes with time in the following.

Figure 5 shows $\mathcal{E} = 1/\tau^2$ at small $A = 0.25$ (top) and large $A = 2.00$ (bottom) for the four radial points $x = 40, 80, 120$, and 160 computed according to Eq. (9). The instances with large values of $\mathcal{E}$ coincides with the sudden change in information length, as expected. In the top panel of Figure 5 for $A = 0.25$, we observe large variation of $\mathcal{E}$ over time for all $x = 40, 80, 120, 160$. However, the blue line ($x = 40$) shows the largest variation, reaching up $\mathcal{E} \sim 6$. This means that for $x = 40$, the potential PDF undergoes a sudden change on a small time scale $\tau \propto \mathcal{E}^{-1/2}$. This behaviour is to be contrasted to the top panel of Figure 1 where there was nothing that distinguishes $x = 40$ from other radial locations $x = 80, 120, 160$ in the time traces. The bottom panel of Figure 5 for $A = 2.0$ also shows that the evolution of $\mathcal{E}$ at $x = 40$ is different from that at other locations. That is, $\mathcal{E}$ helps us identifying and differentiating the behaviour of PDFs at different spatial points. Furthermore, comparing the top ($A = 0.25$) and bottom ($A = 2$) panels of Figure 5, we immediately see a much larger value of $\mathcal{E}$ by almost a factor of 10 for larger $A = 2$. One of the important implications of these results is that a larger adiabaticity increases the likelihood of generation of coherent structures (well known phenomenon in simulations HM plasmas) and that the emergence of these coherent structures is captured by a large value of $\mathcal{E}$, $1/\tau$, or an abrupt change in the slope of the information length.

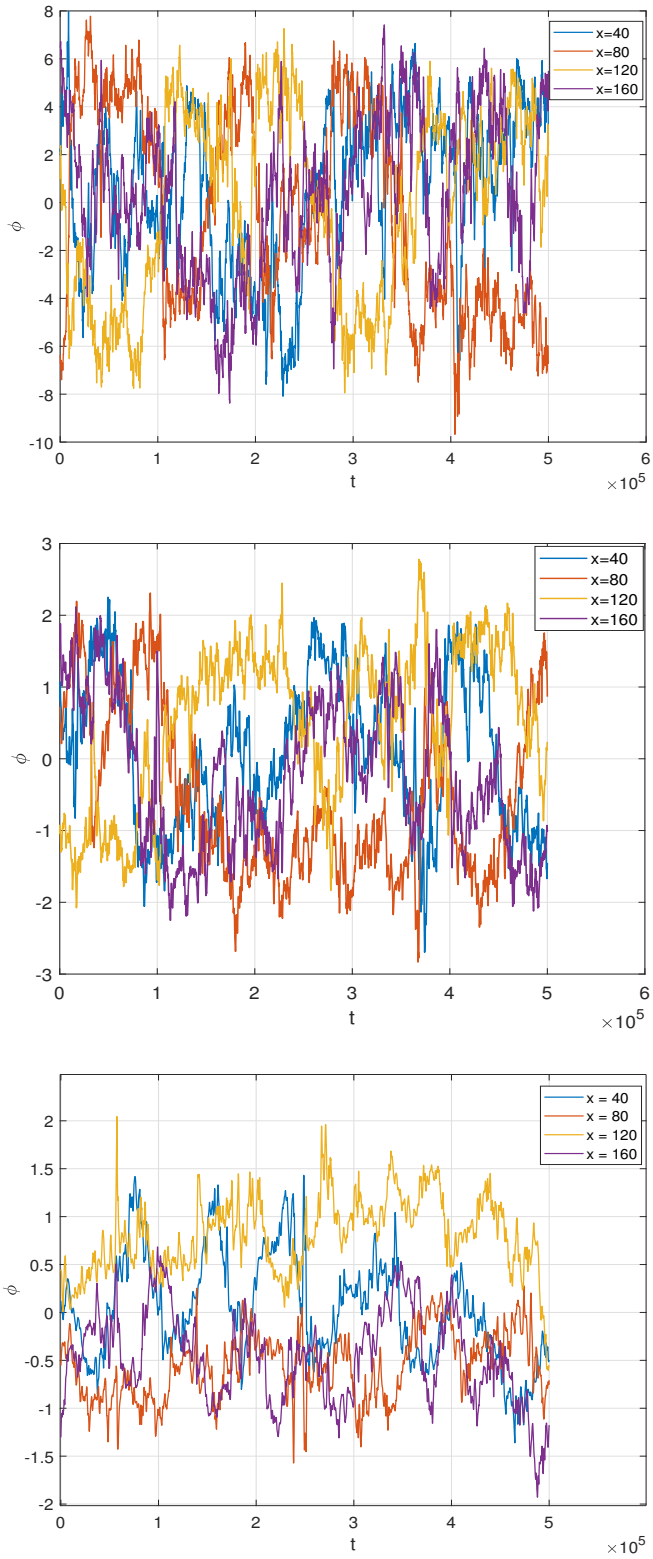

FIG. 1. The time trace of potential at the radial positions (40, 80, 120, 160) for $A = 0.25$ (top), 1.00 (middle) and 2.00 (bottom).

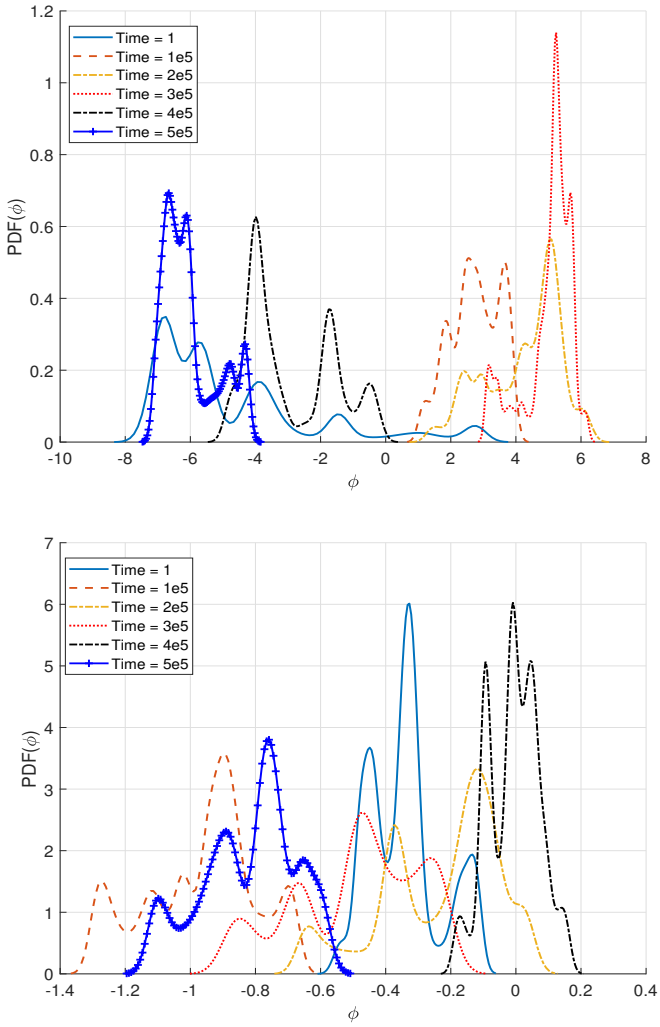

FIG. 2. The time evolution of PDFs of the potential at x = 80 for adiabaticity $A = 0.25$ (top) and $A = 2.00$ (bottom).

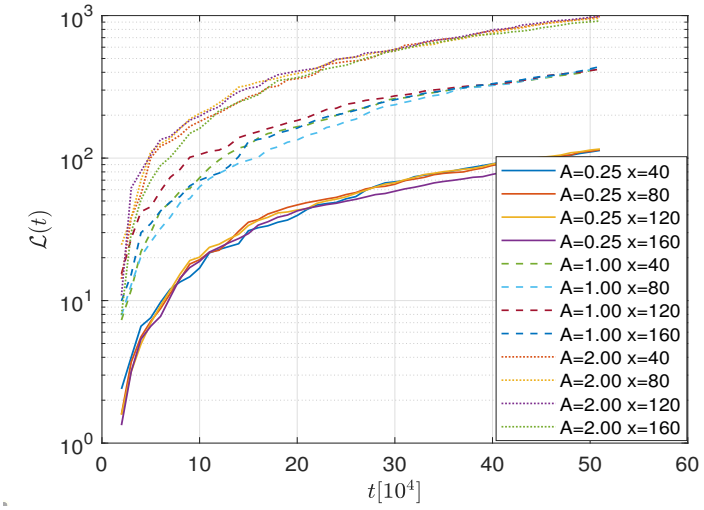

FIG. 3. The logarithm of the information length computed using Eq. (10) for the four radial points and $A = 0.25, 1.00$ and 2.00.

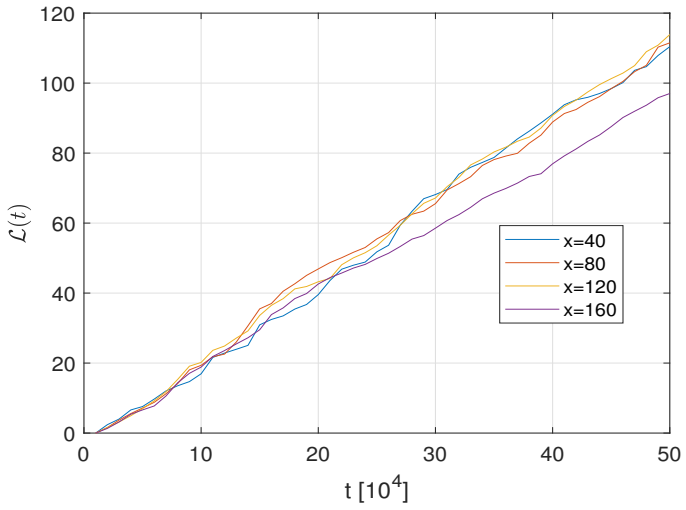

FIG. 4. The information length for small adiabatic index ($A = 0.25$), for the four radial points $x = 40, 80, 120$, and 160.

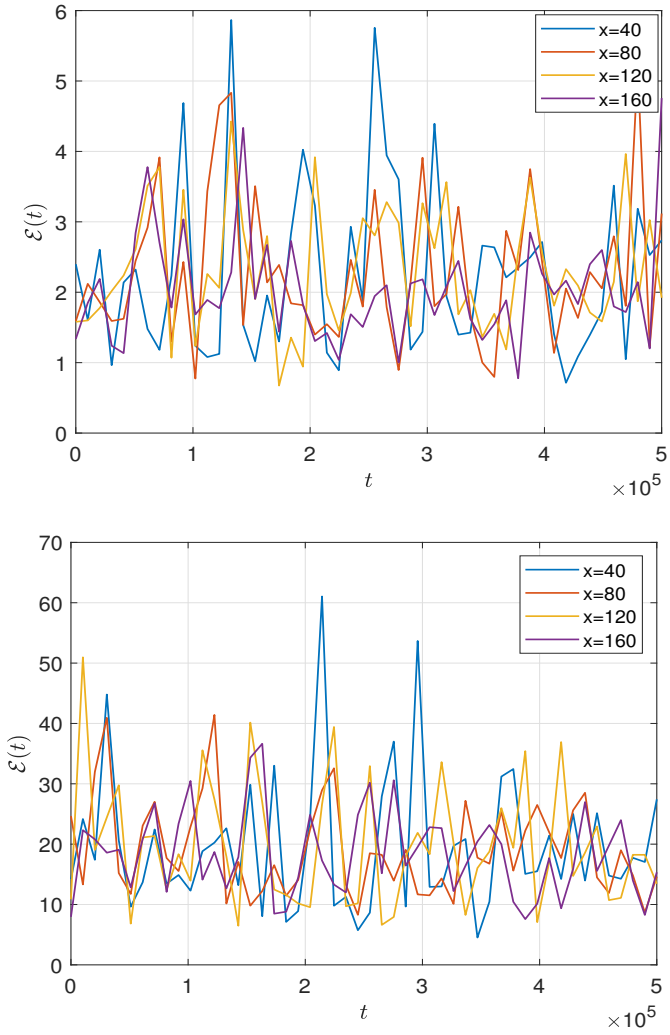

FIG. 5. The dynamic time at small $A = 0.25$ (top) and large $A = 2.00$ (bottom) for the four radial points $x = 40, 80, 120$, and 160.

V. RESULTS FOR VORTICITY WITH VARYING ADIABATICITY

In this section the results for vorticity (zonal component) is presented. First the time traces are shown in Figure 6 and then the information length is displayed in Figure 7. Overall, the time traces of vorticity exhibit similar behaviour to those of the potential where a short time scale oscillation is dominating for small adiabaticity whereas in addition to the short scale oscillations, an oscillation with a longer period emerges for $A = 2.00$. This change in dynamics is also visible in the information length computed according to Eq. (10); the information length increases due to the change in dynamics. Note that the rate of change decreases as a system approaches a quasi-stationary state where the the variation in time-dependent PDFs is small.

The slower variation on a longer time scale, or alternatively, the intermittency due to coherent structures causes abrupt changes in the time evolution of the PDFs, yielding much larger values of information length for a larger adiabaticity A. Furthermore, in comparison with the information length for the potential in Figure (3), Figure (7) shows that as A increases, the information length at different x behaves more differently with a visible separation among different colored lines for a large time. This may be a signature of the effect of coherent structure which decorrelates the vorticity at different x's. Such difference in the information length at different x's is much less clear for the potential itself in Figure (3), in comparison.

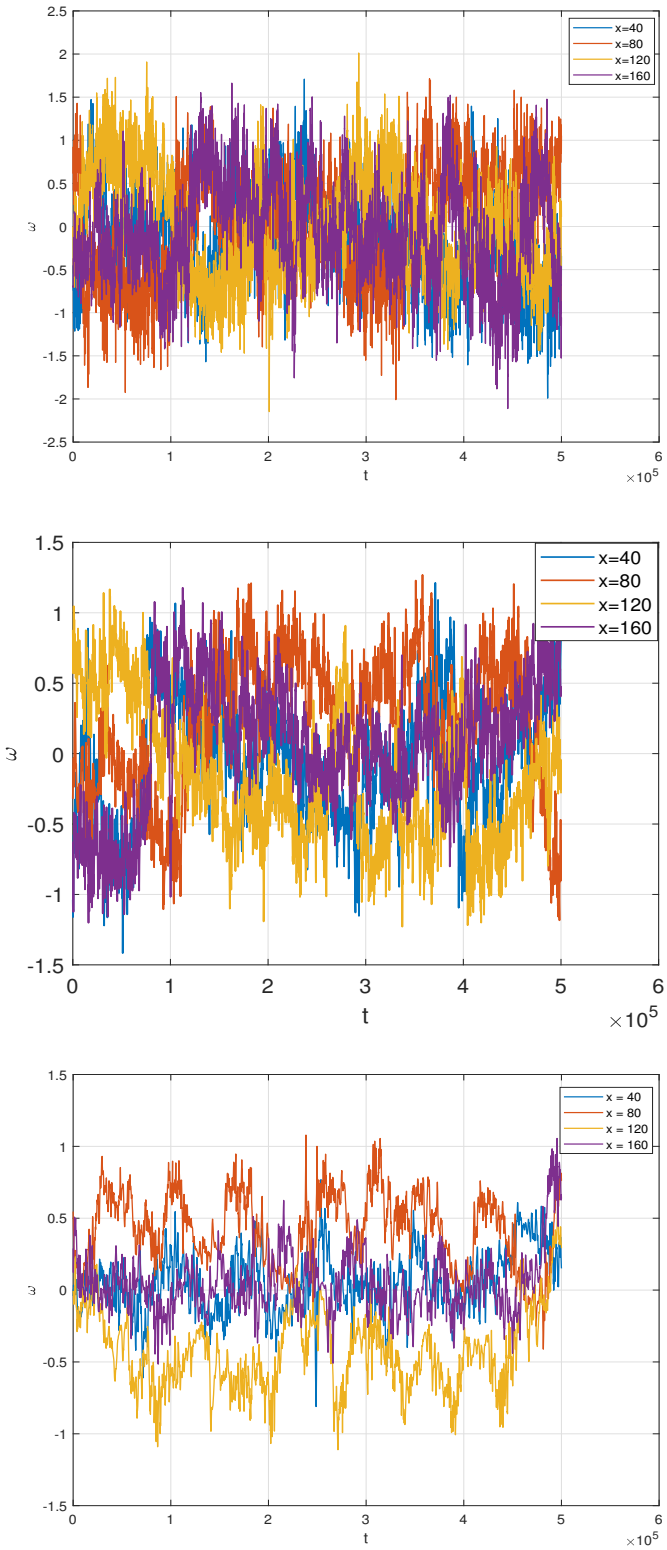

FIG. 6. The time trace of vorticity at the radial positions (40, 80, 120, 160) for $A = 0.25$ (top), 1.00 (middle) and 2.00 (bottom).

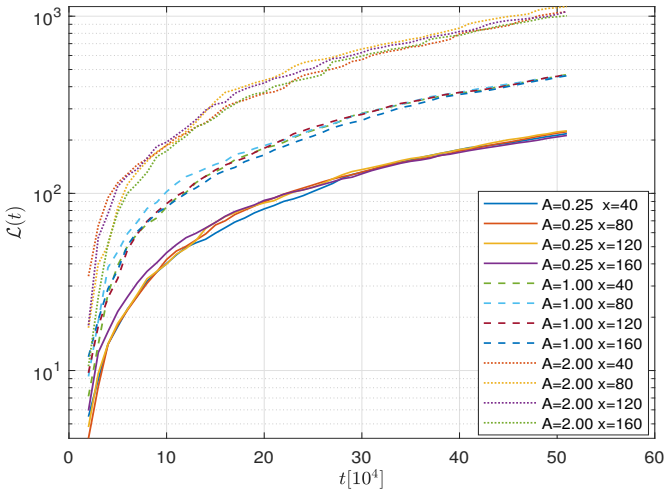

FIG. 7. The logarithm of the information length of vorticity computed using Eq. (10), for the four radial points and $A = 0.25, 1.00$ and 2.00.

VI. RESULTS FOR FLUX WITH VARYING ADIABATICITY

In this section we examine the poloidally averaged density flux, which is calculated by integral (3):

$$\Gamma = \langle \Gamma \rangle = \frac{1}{L_y} \int_0^{L_y} n \frac{\partial \phi}{\partial y} dy. \tag{11}$$

We note that Equation (11) described a second order quantity, i.e. an integral of a product of two fluctuating quantities which thus have unique statistical features different to the statistics of the potential and the density. The three different regimes are elucidated comparing the time traces in Figure (8), and the fast oscillation for small adiabaticity is present whereas the longer time scale fluctuation and intermittency is visible for larger adiabaticity. Note that the fluctuation level is very different with larger fluctuations for smaller adiabaticity. Statistical features of flux time traces have been assessed and discussed previously in Ref. 10.

Of notable in Figure (9) is that as A increases, the information length at different x behaves significantly differently with a large separation among different colored lines. This may be a signature of the effect of coherent structure which reduces the transport in the x-direction, making turbulent statistics different or decorrelated at different x positions. This difference in the information length at different x's is more prominent than that for the vorticity in Figure (7).

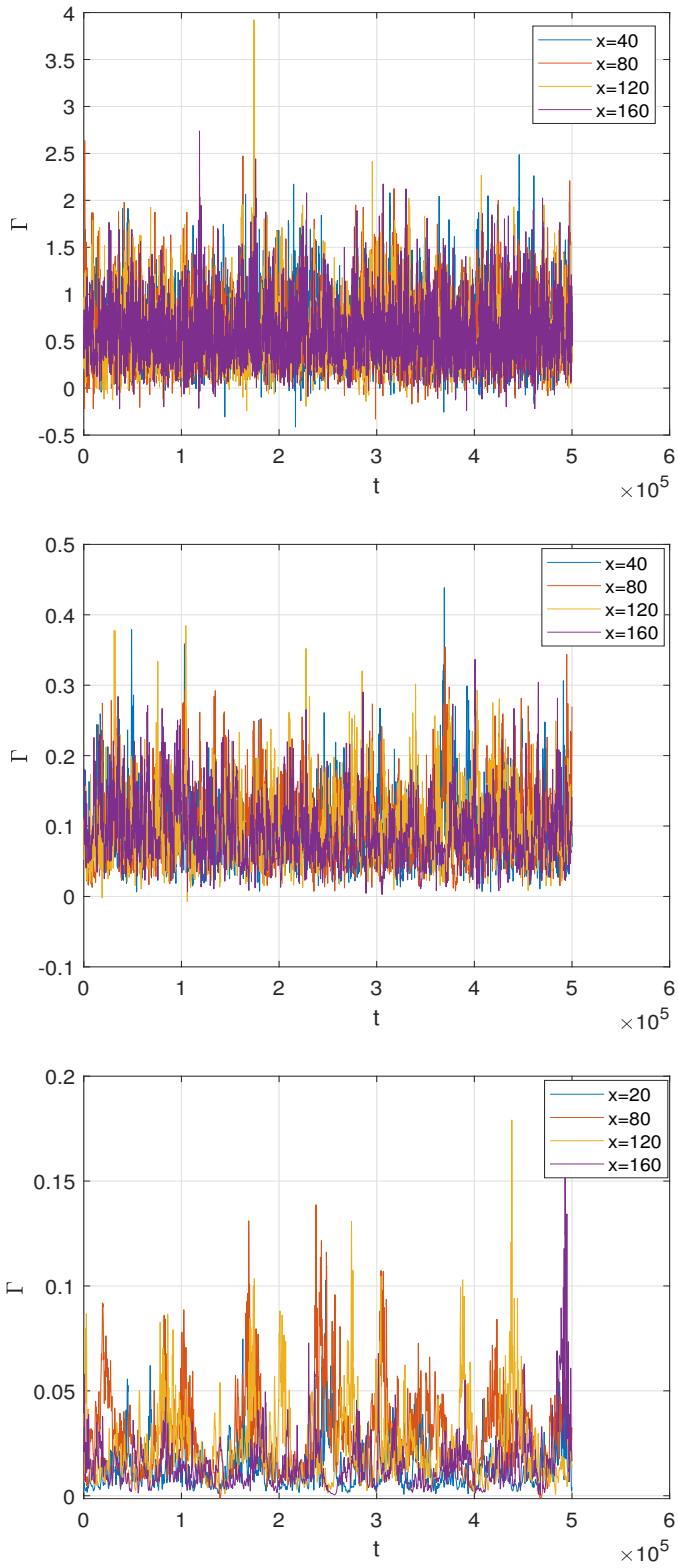

FIG. 8. The time trace of flux at the radial positions (40, 80, 120, 160) for $A = 0.25$ (top), 1.00 (middle) and 2.00 (bottom).

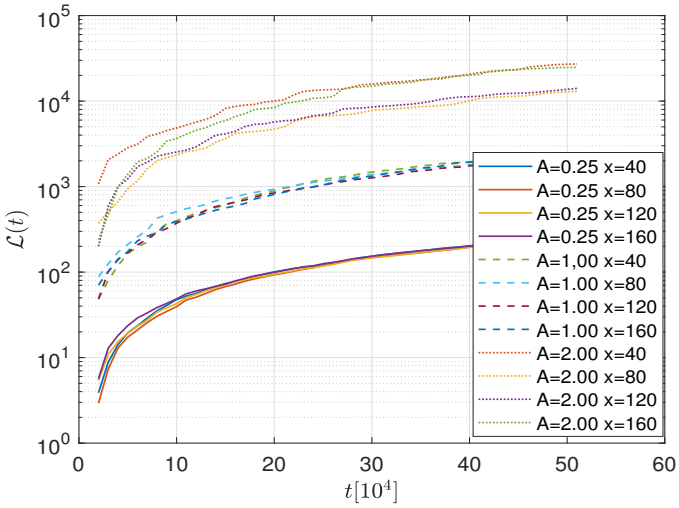

FIG. 9. The logarithm of the information length of flux computed using Eq. (10), for the four radial points and $A = 0.25, 1.00$ and 2.00.

VII. DISCUSSION

The physical understanding of turbulent transport processes has been developed from the Hasegawa - Mima (HM) and Hasegawa - Wakatani (HW) models that include qualitative features and scalings. In this work, we have performed a statistical analysis of the time traces for potential and vorticity generated by fluid like simulations of the HW model. The evolution of the time-dependent probability distribution functions (PDFs) has been analysed by a statistical measure, the so-called information length. The dynamical time τ is a non-negative quantity representing the correlation time over which the (dimensionless) information changes. The information length represents the total different number of states between the initial and final times and establishes a distance between the initial and final PDFs in the statistical space along a path of a system.

Specifically, we calculated the time traces of the potential and density and analyzed the poloidally averaged simulation data at ten radial positions and three different adiabaticity index $A = 0.25, 1, 2$. The modified HW model with periodic boundary conditions is radially homogeneous however at the same time yield a zonal flow dominated state which significantly influences the averages and thus the PDFs.

However for simplicity, in the figures, the results were shown only for the positions $x = 40, 80, 120$ and 160. The simulation length is 500 001 time steps where the PDFs were constructed using $t = 10000$ time steps where one PDF per 100 000 time steps was shown. We observed a variation in mean and variance of the PDFs as time progressed, see e.g. Figures 1 and 6. The expression in (9) is non-negative and thus the information length which is the time integral is a nondecreasing function of time; see e.g. Figures 3, 7 and 9. In fact, the information length could almost linearly increase with time but with large fluctuations. Note that the time trace of vorticity was varying faster than the potential, leading to a larger information length for the vorticity than for the potential.

Moreover, there is a distinct difference between $A = 0.25$ and $A = 2.00$ cases due to the difference in dynamics, for $A = 0$ the system reduces to the Euler equation. The oscillations (on a fast and a slower time scale) in time give rise to PDFs that are localized at different values of potential ϕ or vorticity ω. Overall, a smaller A leads to a smaller

information length due to large fluctuation (uncertainty). This signifies that intermittency due to coherent structures causes abrupt changes in the time evolution of the PDFs, yielding much larger values of information length for a larger adiabaticity A.

It is worth noting that one of the signature of transport caused by coherent structures is elevated tails in comparison with the Gaussian distribution. It is found that the statistics of quantities describing transport mediated by coherent structures exhibits non-Gaussian features and has significantly increased kurtosis (Kurtosis is the normalized fourth moment, where a Gaussian process has a kurtosis of 3.), for instance, as shown in the previous work in Ref. 10.

In the paper, we have demonstrated that the information length provides an alternative methodology to understand the effect of coherent structures on transport and intermittency. Specifically, the information length or the dynamic time τ was shown to be a useful diagnostics for accessing large events, or intermittent transport due to coherent structures. We also have shown that the information length can quantify the decorrelation of the flux between different spatial (x) positions due to coherent structure.

In conclusion, our model was chosen for the reasons that it inherently includes coherent structures and qualitatively describes the complex plasma dynamics in magnetically confined plasmas. The information length was shown to be a novel methodology of assessing the effects of coherent structures and turbulent dynamics in plasmas. It is feasible to generate a plasma fluid simulation containing many turnover times of the turbulent process such that the time traces can be expected to exhibit enough information for this type of analysis. The results suggest that this opens a new promising field of application of information length. In particular, it is feasible to find changes in the dynamics as a sudden change in distance between PDFs assessed by the information space, thus it could be a valuable tool for the investigation of turbulent plasma dynamics.

REFERENCES

[1]W. Horton, Rev. Mod. Phys. **71**, 735 (1999).

[2]A. Hasegawa and K. Mima, Phys. Rev. Lett. **39**, 205 (1977).

[3]A. Hasegawa and K. Mima, Phys. Fluids, **21**, 87 (1978).

[4]A. Hasegawa, C. G. Maclennan and Y. Kodama, Phys. Fluids, **22**, 2122 (1979).

[5]A. Hasegawa and M. Wakatani, Phys. Rev. Lett. **50**, 682 (1983).

[6]A. Hasegawa and M. Wakatani, Phys. Rev. Lett. **59**, 1581 (1986).

[7]J. M. Dewhurst, B. Hnat, N. Ohno, R. O. Dendy, S. Masuzaki, T. Morisaki and A. Komori, Plasma Phys. Contr. Fusion **50**, 095013 (2008).

[8]J. M. Dewhurst, B. Hnat and R. O. Dendy, Phys. Plasmas **16**, 072306 (2009).

[9]T. Stoltzfus-Dueck, B. D. Scott and J. A. Krommes, Phys. Plasmas **20**, 082314 (2013).

[10]J. Anderson and B. Hnat, Physics of Plasmas **24** (6), 062301 (2017).

[11]W. Horton and Y.-H. Ichikawa, *Chaos and Structures in Nonlinear Plasmas* (World Scientific, Singapore, 1996), Sections 6.1 & 6.2, p.221.

[12]S. Zweben, J. A. Boedo, O. Grulke, C. Hidalgo, B. LaBombard, R. J. Maqueda, P. Scarin and J. L. Terry, Plasma Phys. Contr. Fusion **49**, S1 (2007).

[13]P. A. Politzer, Phys. Rev. Lett. **84**, 1192 (2000).

[14]P. Beyer, S. Benkadda, X. Garbet and P. H. Diamond, Phys. Rev. Lett. **85**, 4892 (2000).

[15]J. F. Drake, P. N. Guzdar and A. B. Hassam, Phys. Rev. Lett. **61**, 2205 (1988).

[16]G. Y. Antar, S. I. Krasheninnikov, P. Devynck, R. P. Doerner, E. M. Hollman, J. A. Boedo, S. C. Luckhardt and R. W. Conn, Phys. Rev. Lett. **87**, 065001 (2001).

[17]B. A. Carreras, C. Hidalgo, E. Sanchez, M. A. Pedrosa, R. Balbin, I. Garcia-Cortes, B. van Milligen. D. E. Newman and V. E. Lynch, Phys. Plasmas **3**(7),(1996).

[18]J. Anderson and P. Xanthopoulos, Phys. Plasmas **17**, 110702 (2010).

[19]E. Kim and J. Anderson, Phys. Plasmas **15**, 114506 (2008).

[20]J. Anderson, E. Kim and S. Moradi, Phys. Plasmas, **21**, 122109 (2014).

[21]J. Anderson, S. Moradi, T. Rafiq, Entropy, 20(10), 760 (2018).

[22]P. H. Diamond, S.-I. Itoh, K. Itoh and T. S. Hahn, Plasma Phys. Contr. Fusion **47**, R35 (2005).

[23]J. W. Connor, T. Fukuda, X. Garbet, C. Gormezano, V. Mukhovatov, M. Wakatani, the ITB Database Group and the ITPA Topical Group on Transport and Internal Barrier Physics, Nucl. Fusion **44**, R1 (2004).

[24]K. Itoh, S.-I. Itoh, P. H. Diamond, T. S. Hahn, A. Fujisawa, G. R. Tynan, M. Yagi and Y. Nagashima, Phys. Plasmas **13**, 055502 (2006).

[25]J. W. Connor and T. J. Martin, Plasma Phys. Contr. Fusion **49**, 1497 (2007).

[26]F. Weinhold, Z. Phys. Chem., **63**, 2479 (1975).

[27]G. Rupeiner, Phys. Rev. Lett. **20**, 1608 (1979).

[28]F. Schlögl, Z. Phys. B **59**, 449–454 (1985).

[29]L. Diósi, K. Kulacsy, B. Lukács, A. Rácz, Z. Phys. Chem. **105** 11220 (1996).

[30]G. E. Crooks, Phys. Rev. Lett. **99** 100602 (2007).

[31]E. H. Feng, G. E. Crooks, Phys. Rev. E **79** 012104 (2009).

[32]S. B. Nicholson, E. Kim, Phys. Lett. A **379** 83 (2015).

[33]E. Kim and R. Hollerbach, Phys. Rev. E **95**, 022137 (2017).

[34]E. Kim and R. Hollerbach, Phys. Rev. E **95**, 062107 (2017).

[35]E. Kim, Q. Jacquet and R. Hollerbach, J. Stat. Mech., 023204 (2019).

[36]E. Kim, Entropy **20** (8), 574 (2018).

[37]J. Heseltine & E. Kim, Entropy **21** (8), 775 (2019).

[38]R. Hollerbach E. Kim, Entropy **19**, 268, e19060268 (2017).

[39]E. Kim, L.-M. Tenkes, R. Hollerbach and Ovidiu Radulescu, Entropy **19**, 511, e19100511 (2017).